2011 50th IEEE Conference on Decision and Control and
European Control Conference (CDC-ECC)
Orlando, FL, USA, December 12-15, 2011

Formation Control with Collision Avoidance

Ricardo Bencatel, Mariam Faied, João Sousa, and Anouck R. Girard

Abstract— **We present a formation flight control strategy featuring a collision avoidance scheme. The control algorithm is based on a Sliding Mode controller. The controller sliding surfaces account for aircraft maneuvering limitations, restricting the required velocities to a feasible set. Further, the relative position between vehicles affects the sliding surfaces shape, enabling collision avoidance. The control method derivation is based on an extended unicycle model, resulting in a controller adequate for fixed wing aircraft.**

I. INTRODUCTION

Formation flight is an interesting topic in aircraft control as it presents the challenge of interconnected systems [1]. Some applications include air refueling, forest fire mapping [2], radar deception, distributed sensing [3], fuel saving [4], [5], transportation [6], [7], communication networks [8], and more. For atmospheric data sampling [3] in particular, formation flight allows us to gather spatially distributed measurements simultaneously.

A. General Problem

The formation flight control problem is dominated by the issue of forcing a relative position among aircraft. Further, there are two other important issues in formation control: bringing the formation together and avoiding any collision.

B. Literature Review

Zheng et al. [9] derived a Sliding Mode controller for a leaderless formation and applied it to a group of holonomic vehicles. This method was tested with ground robots with good results. Sharifi et al. [10] present a decentralized sliding mode control method for a leader formation with communication delays. This study shows how the decentralized controller on one vehicle predicts other vehicles' dynamics and how this improves formation stability. Gu et al. [11] designed a leader formation control method and flight tested it with two YF-22 models. Tests showed that the follower is able to track its formation position safely. The main requirements are that the flight condition remains near the one used for the controller parameter estimation and that the system starts from the same quadrant as the desired position relative to the leader. SMAVNET project proved the feasibility of safe formation flight up to 10 aircraft. The collision avoidance system is described by Leven et al. in [12]. Waydo et al. [13] implemented and tested a formation control system based on receding horizon control (RHC) supervised by a high level controller. The control scheme was simulated and flight tested with the X-35A avionics mounted on an adapted T-33 jet trainer, following an F-15 fighter jet. The whole control protocol was provably safe. This was achieved as the aircraft dynamics, RHC dynamics, and the supervisor controller where described and specified with temporal logic, which allowed the authors to prove the desired properties.

Aircraft collision avoidance is a complex problem in normal flight as well as in formation flight. Tomlin et al. [14] studied multiagent conflicts under a hybrid systems framework. They describe a method based on Hamilton-Jacobi-Isaacs PDE to generate conflict resolution trajectories that are provably safe for two aircraft. This method computes the reachable set of the hybrid system accounting for vehicles nonlinear dynamics and the intent uncertainty of one of the aircraft.

The formation stability problem was addressed by Swaroop et al. in [15]. It was proved that interconnected systems are stable in the vicinity of the equilibrium point if they are loosely coupled and the individual systems are exponentially stable. NASA also studied the problem of string stability of their F/A-18 formation control system. Allen et al. [16] concluded that although the control system was string unstable it was applicable to a bounded number of aircraft as the position oscillation was limited by an acceptable range.

C. Current Approach

This work extends the formation Sliding Mode Controller (SMC) presented by Zheng et al. [9]. This study is constrained to the horizontal plane for simplicity. However, it is applicable to 3D formations with few adjustments. The main contributions are the inclusion of a collision avoidance scheme in the control system definition, the use of an extended unicycle dynamic model for the SMC derivation, and the incorporation of maneuvering restrictions on the sliding surfaces. The SMC derivation based on the extended unicycle model (section II-A) creates a controller with dynamics adequate for fixed wing aircraft control. The SMC is defined for each aircraft and includes a set of two sliding surfaces for each of the other interacting aircraft (section II-B). The sliding surfaces shapes and magnitudes restrict the maximum commanded velocities to the aircraft limits.

In the solution presented by Zheng et al., there was a gain which controlled relative importance between the formation shape and each vehicle position error in the formation. The present solution has a similar gain which defines the relative

The research leading to this work was funded by *Financiamento plurianual* of the *FEUP ISR Porto* R&D unit and by the *FCT* (Foundation for Science and Technology) under PhD grant *SFRH/BD/40764/2007*.

R. Bencatel and J. Sousa are with the Department of Electrical and Computer Engineering, School of Engineering, University of Porto, 4200 Porto, Portugal (ricardo.bencatel@fe.up.pt)

A. Girard and M. Faied are with the Department of Aerospace Engineering, University of Michigan, Ann Arbor, MI 48109, USA

importance between the formation shape and leader-relative position error, i.e., the deviation from its desired position relative to the leader (section II-B.4).

We implemented some logic to force the collision avoidance dynamics, which are described in section II-B.2.

This method was developed to be implemented on fixed wing Unmanned Air Vehicles (UAVs). The current approach holds the leader as a non-collaborative agent with some dynamic restrictions. It flies as if it was alone, defining the formation path, through its speed and turn rate. Its speed and turn rate are limited to a range conducive to feasible paths by every formation aircraft. Currently, the method does not account for fixed obstacles or adversary agents.

In terms of communications, this method requires that all interacting aircraft, including the leader, broadcast their horizontal position, velocity, and acceleration. Every follower aircraft requires the data about its and every other aircraft's desired position, velocity and acceleration in the formation, and every other aircraft's current horizontal position, velocity, and acceleration.

II. Leader formation control

A. 2D Motion Model

The *2D motion* model simulates an airplane, in which the autopilot forces coordinated turns (zero side-slip) at constant altitude. The airspeed (V_a) and roll (ϕ) are regarded as the autopilot pseudo-controls. Further, we assume a nearly null angle of attack and that the autopilot provides a higher bandwidth regulator for the roll angle, making its dynamics negligible when compared to the heading dynamics. The planar motion of the airplane is simulated by a simple 3 Degrees-of-Freedom (DOF) kinematic model. The model described next is an extension of a unicycle model.

$$\dot{x} = V_a \cdot \cos(\psi) + W_x = V_g \cdot \cos(\chi) \tag{1a}$$

$$\dot{y} = V_a \cdot \sin(\psi) + W_y = V_g \cdot \sin(\chi) \tag{1b}$$

$$\dot{\psi} = \omega = \frac{g \cdot \tan(\phi)}{V_g}, \tag{1c}$$

where V_a and V_g are the air-relative and ground-relative velocities, also designated as airspeed and ground speed, respectively. χ is the course angle, i.e., the direction the aircraft is actually following. W_x and W_y are the wind velocity components on the x and y axis.

B. Sliding Mode Controller

In this approach to formation flight we use Sliding Mode Control. In a formation with N UAVs, each UAV has $N-1$ inter-UAV reference frames (fig. 1). Each inter-UAV reference frame is centered on a UAV i center of mass (CM), with the $\hat{\mathbf{x}}_{ij}$ axis pointing to UAV j CM, and $\hat{\mathbf{y}}_{ij}$ axis rotated clockwise in the horizontal plane. ψ_{ij} is the deviation of $\hat{\mathbf{x}}_{ij}$ from the fixed frame $\hat{\mathbf{x}}_f$ axis. Two sets of sliding surfaces are implemented. Each sliding surface implements a different strategy on each inter-UAV frame axis (fig. 1). A *MaxVel* strategy is applied on the $\hat{\mathbf{y}}_{ij}$ axis to regulate error position on that same axis. This strategy gets its name from the full speed command with large position errors. A collision avoidance strategy is applied on the $\hat{\mathbf{x}}_{ij}$ axis for collision avoidance and to regulate position error on that axis.

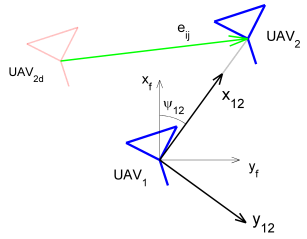

Fig. 1: Inter-UAV relative frame

$$\hat{\mathbf{x}}_{ij} = [\cos(\psi_{ij}) \ \sin(\psi_{ij})]^\mathsf{T} \tag{2a}$$

$$\hat{\mathbf{y}}_{ij} = [-\sin(\psi_{ij}) \ \cos(\psi_{ij})]^\mathsf{T} \tag{2b}$$

$$\psi_{ij} = \tan^{-1}\left(\frac{y_j - y_i}{x_j - x_i}\right) \tag{2c}$$

1) MaxVel sliding surface: The *MaxVel* surface equation is presented here,

$$S = v + c_1 \cdot \mathrm{sgn}(x) - \frac{c_2}{x + c_3 \cdot \mathrm{sgn}(x)} \tag{3a}$$

$$\dot{S} = \dot{v} + \frac{c_2 \cdot \dot{x}}{(x + c_3 \cdot \mathrm{sgn}(x))^2}. \tag{3b}$$

$c_1 = V_{max}$ is set such that the commanded velocity doesn't exceed the maximum allowed velocity. The constants c_2 and c_3 are calibration variables and will be defined below.

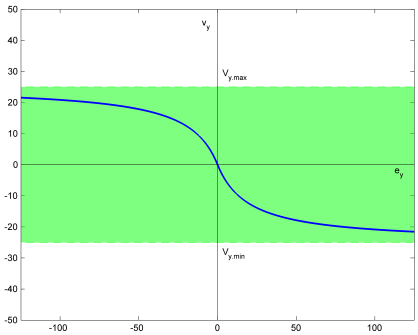

Fig. 2: Standard position tracking sliding surface

2) Collision avoidance sliding surface: On the $\hat{\mathbf{x}}_{ij}$ axis, which "connects" both UAVs, we desire a repelling behavior. If the UAVs are at a distance $\Delta x \leq r_{min}$, the velocity of each UAV should be maximum in the opposite direction relative to the other UAV, where r_{min} is the *safety distance*. If the UAVs are at a distance $\Delta x \leq r_d \Rightarrow v_x \in [-V_{max}, 0]$, where r_d is the relative desired distance. This means that the UAVs relative distance should still increase. If the UAVs are at a distance $\Delta x \geq r_d \Rightarrow v_x \in [0, V_{max}]$, which means that the UAVs relative distance should decrease. This also implies that the commanded velocity will not exceed V_{max} when the UAVs are far away. We defined the sliding surface

as an offset inverse function of velocity error *vs* position error (fig. 3). The desired behavior is implemented by the

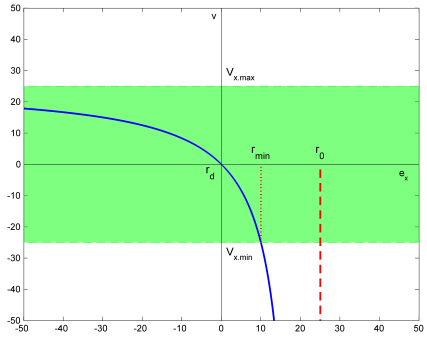

Fig. 3: Collision avoidance sliding surface

following sliding surface:

$$S = v + c_1 - \frac{c_2}{x + c_3} \tag{4a}$$

$$c_1 = V_{max}, c_2 = 2V_{max}\left(r_d - r_{min}\right) \wedge c_3 = 2\left(r_d - r_{min}\right)$$

$$\dot{S} = \dot{v} + \frac{c_2 \cdot \dot{x}}{\left(x - c_3\right)^2} \tag{4b}$$

3) Formation controller: The complete system behavior can be obtained by a weighted sum of the individual sliding surfaces projected on the Earth frame. This is defined by an $\hat{\mathbf{x}}_f$ axis pointing North and a $\hat{\mathbf{y}}_f$ axis pointing East, centered on a fixed point over the ground surface.

$$\mathbf{s}_{Fi} = \sum_{j \neq i}^{N} \mathbf{s}_{ij} \tag{5}$$

$$\mathbf{s}_{ij} = \left[\dot{e}_{x.ij} + c_1 - \frac{c_2}{e_{x.ij} + c_3}\right]\hat{\mathbf{x}}_{ij} + \\ + \left[\dot{e}_{y.ij} + c_1 \cdot \operatorname{sgn}\left(e_{y.ij}\right) - \frac{c_2}{e_{y.ij} + c_3 \cdot \operatorname{sgn}\left(e_{y.ij}\right)}\right]\hat{\mathbf{y}}_{ij} \tag{6}$$

where $e_{x.ij}$ and $e_{y.ij}$ are the position errors projected on the inter-UAV frame, as

$$\mathbf{e}_{ij} = \mathbf{x}_i - \mathbf{x}_j - \Delta\mathbf{x}_{d.ij} \tag{7a}$$

$$e_{x.ij} = \mathbf{e}_{ij} \cdot \hat{\mathbf{x}}_{ij} \tag{7b}$$

$$e_{y.ij} = \mathbf{e}_{ij} \cdot \hat{\mathbf{y}}_{ij} \tag{7c}$$

$$\boldsymbol{R}_{\psi_{ij}} = \begin{bmatrix} \hat{\mathbf{x}}_{ij}^{\intercal} \\ \hat{\mathbf{y}}_{ij}^{\intercal} \end{bmatrix} = \begin{bmatrix} \cos\left(\psi_{ij}\right) & \sin\left(\psi_{ij}\right) \\ -\sin\left(\psi_{ij}\right) & \cos\left(\psi_{ij}\right) \end{bmatrix} \tag{7d}$$

$\boldsymbol{R}_{\psi_{ij}}$ is the rotation matrix from the Earth frame to the inter-UAV frame, $\Delta\mathbf{x}_{d.ij} = \mathbf{x}_{d.i} - \mathbf{x}_{d.j}$, and $\|\Delta\mathbf{x}_{d.ij}\| = r_d$. The formation desired positions for each vehicle i are defined by the system operator through the vector $\mathbf{x}_{d.i}^{F} = [x_{i.F}, y_{i.F}]^{\intercal}$ in the formation reference frame (defined in sections II-C and II-D).

With the definitions in (7) we may simplify (6) by merging $\dot{e}_{x.ij}\hat{\mathbf{x}}_{ij}$ and $\dot{e}_{y.ij}\hat{\mathbf{y}}_{ij}$ into $\dot{\mathbf{e}}_{ij}$, resulting in:

$$\mathbf{s}_{ij} = \dot{\mathbf{e}}_{ij} + \left[c_1 - \frac{c_2}{e_{x.ij} + c_3}\right]\hat{\mathbf{x}}_{ij} + \\ + \left[c_1 \cdot \operatorname{sgn}\left(e_{y.ij}\right) - \frac{c_2}{e_{y.ij} + c_3 \cdot \operatorname{sgn}\left(e_{y.ij}\right)}\right]\hat{\mathbf{y}}_{ij} \tag{8}$$

As the control vector has no direct effect in (5) we derive it:

$$\mathbf{s}_{Fi} = \sum_{j \neq i}^{N}\left[\dot{\mathbf{e}}_{ij} + \left(c_1 - \frac{c_2}{e_{x.ij} + c_3}\right)\hat{\mathbf{x}}_{ij} + \\ + \left(c_1 \cdot \operatorname{sgn}\left(e_{y.ij}\right) - \frac{c_2}{e_{y.ij} + c_3 \cdot \operatorname{sgn}\left(e_{y.ij}\right)}\right)\hat{\mathbf{y}}_{ij}\right] \tag{9}$$

$$\dot{\mathbf{s}}_{Fi} = \sum_{j \neq i}^{N}\left(\ddot{\mathbf{e}}_{ij} + \varepsilon_{ij}\right), \tag{10}$$

where ε_{ij} is the pseudo error rate, defined as:

$$\varepsilon_{ij} := \left(\frac{c_2 \cdot \dot{e}_{x.ij}}{\left(e_{x.ij} + c_3\right)^2} - c_1 \cdot \dot{\psi}_{ij} \cdot \operatorname{sgn}\left(e_{y.ij}\right) + \right. \\ + \frac{c_2 \cdot \dot{\psi}_{ij}}{e_{y.ij} + c_3 \cdot \operatorname{sgn}\left(e_{y.ij}\right)}\Bigg)\hat{\mathbf{x}}_{ij} + \\ + \left(\frac{c_2 \cdot \dot{e}_{y.ij}}{\left(e_{y.ij} + c_3 \cdot \operatorname{sgn}\left(e_{y.ij}\right)\right)^2} + \right. \\ \left. + c_1 \cdot \dot{\psi}_{ij} - \frac{c_2 \cdot \dot{\psi}_{ij}}{e_{x.ij} + c_3}\right)\hat{\mathbf{y}}_{ij}, \tag{11}$$

From equation (7) we can derive,

$$\dot{\mathbf{e}}_{ij} = \dot{\mathbf{x}}_i - \dot{\mathbf{x}}_j - \dot{\Delta\mathbf{x}}_{d.ij},\ \ddot{\mathbf{e}}_{ij} = \ddot{\mathbf{x}}_i - \ddot{\mathbf{x}}_j - \ddot{\Delta\mathbf{x}}_{d.ij} \tag{12a}$$

$$\dot{e}_{x.ij} = \dot{\mathbf{e}}_{ij} \cdot \hat{\mathbf{x}}_{ij} + \mathbf{e}_{ij} \cdot \hat{\mathbf{y}}_{ij}\dot{\psi}_{ij} \tag{12b}$$

$$\dot{e}_{y.ij} = \dot{\mathbf{e}}_{ij} \cdot \hat{\mathbf{y}}_{ij} - \mathbf{e}_{ij} \cdot \hat{\mathbf{x}}_{ij}\dot{\psi}_{ij} \tag{12c}$$

$$\dot{\psi}_{ij} = \frac{\left(\dot{\mathbf{x}}_j - \dot{\mathbf{x}}_i\right) \cdot \hat{\mathbf{y}}_{ij}}{\|\boldsymbol{\Delta}\mathbf{x}_{ij}\|} \tag{12d}$$

The desired acceleration, by derivation of (1), is

$$\ddot{\mathbf{x}}_i = \begin{bmatrix} \cos\left(\psi_i\right) & -V_{a.i} \cdot \sin\left(\psi_i\right) \\ \sin\left(\psi_i\right) & V_{a.i} \cdot \cos\left(\psi_i\right) \end{bmatrix}\begin{bmatrix} \dot{V}_{a.i} \\ \dot{\psi}_i \end{bmatrix} + \\ + \begin{bmatrix} \dot{W}_x \\ \dot{W}_y \end{bmatrix}_i = \mathbf{A}_i\nu_i + \dot{\mathbf{w}}_i,\ i = 1, ..., N, \tag{13}$$

where ν_i is the *i*th aircraft control vector and $\dot{\mathbf{w}}_i$ is the *i*th aircraft local flow variation.

Merging equations (10) and (13) and rearranging, we obtain:

$$\dot{\mathbf{s}}_{Fi} = \sum_{j \neq i}^{N}\left(\boldsymbol{A}_i\nu_i + \dot{\mathbf{w}}_i - \boldsymbol{A}_j\nu_j - \dot{\mathbf{w}}_j - \ddot{\Delta\mathbf{x}}_{d.ij} + \varepsilon_{ij}\right). \tag{14}$$

We can select ν_i such that the known terms are cancelled,

$$\nu_i = \frac{\boldsymbol{A}_i^{-1}}{N-1}\left[\sum_{j \neq i}^{N}\left(\boldsymbol{A}_j\nu_j + \ddot{\Delta\mathbf{x}}_{d.ij} - \varepsilon_{ij}\right) + \tilde{\nu}_i\right], \tag{15}$$

where $\tilde{\nu}_i$ is the ith aircraft pseudo control vector, and yielding:

$$\dot{\mathbf{s}}_{Fi} = \tilde{\nu}_i + \sum_{j \neq i}^{N} \left(\dot{\mathbf{w}}_i - \dot{\mathbf{w}}_j \right). \tag{16}$$

To force the system to converge to the sliding surface we define a Lyapunov function candidate of the form $V = S^2$, yielding $\dot{V} = 2S\dot{S}$. To ensure formation stability about the desired positions, $\dot{V}$ needs to be negative definite, and so $S\dot{S} < 0$:

$$\mathbf{s}_{Fi} \cdot \dot{\mathbf{s}}_{Fi} = \mathbf{s}_{Fi} \cdot \left[\tilde{\nu}_i + \sum_{j \neq i}^{N} \left(\dot{\mathbf{w}}_i - \dot{\mathbf{w}}_j \right) \right]. \tag{17}$$

If the uncertainty of $\dot{\mathbf{w}}$ is bounded we can assume a worst-case scenario:

$$\|\dot{\mathbf{w}}_i\| \leq \dot{w}_{max},\ i = 1, ..., N \tag{18a}$$

$$\dot{\mathbf{w}}_i - \dot{\mathbf{w}}_j \leq 2\dot{w}_{max} \mathrm{sgn}\left(\mathbf{s}_{Fi}\right) = 2\dot{w}_{max} \frac{\mathbf{s}_{Fi}}{\|\mathbf{s}_{Fi}\|} \tag{18b}$$

$$\mathbf{s}_{Fi} \cdot \dot{\mathbf{s}}_{Fi} \leq \mathbf{s}_{Fi} \cdot \left[\tilde{\nu}_i + 2\left(N-1\right) \dot{w}_{max} \mathrm{sgn}\left(\mathbf{s}_{Fi}\right) \right]. \tag{18c}$$

As we need to assure $\mathbf{s}_{Fi} \cdot \dot{\mathbf{s}}_{Fi} < 0$, we force $\mathbf{s}_{Fi} \cdot \left[\tilde{\nu}_i + 2\left(N-1\right) \dot{w}_{max} \mathrm{sgn}\left(\mathbf{s}_{Fi}\right) \right] < 0$ with:

$$\tilde{\nu}_i = -\left[\Lambda \mathrm{sat}\left(\frac{\mathbf{s}_{Fi}}{\Phi} \right) + 2\left(N-1\right) \dot{w}_{max} \mathrm{sgn}\left(\mathbf{s}_{Fi}\right) \right], \tag{19}$$

where

$$\mathrm{sat}\left(\frac{\mathbf{s}_{Fi}}{\Phi} \right) = \begin{cases} \frac{\mathbf{s}_{Fi}}{\Phi} & \|\mathbf{s}_{Fi}\| < \Phi \\ \frac{\mathbf{s}_{Fi}}{\|\mathbf{s}_{Fi}\|} & otherwise \end{cases}. \tag{20}$$

$\mathbf{s}_{Fi} \cdot \dot{\mathbf{s}}_{Fi} \leq -\mathbf{s}_{Fi} \cdot \Lambda \mathrm{sat}\left(\frac{\mathbf{s}_{Fi}}{\Phi}\right) < 0$ is guaranteed if Λ is a positive definite matrix. The control vector is then,

$$\nu_i = \frac{\boldsymbol{A}_i^{-1}}{N-1} \left[\sum_{j \neq i}^{N} \left(\boldsymbol{A}_j \nu_j + \ddot{\Delta}\mathbf{x}_{d.ij} - \varepsilon_{ij} \right) - \Lambda \mathrm{sat}\left(\frac{\mathbf{s}_{i,F}}{\Phi} \right) - \right.$$
$$\left. -2\left(N-1\right) \dot{w}_{max} \mathrm{sgn}\left(\mathbf{s}_{Fi}\right) \right] \tag{21}$$

4) Leader Effector: The user may tune the balance between the shape stiffness and the regulation of the positional error relative to the leader. This is controlled through an increased gain of the leader over the formation controls (21):

$$\nu_i = \frac{\boldsymbol{A}_i^{-1}}{N-1+k_L} \left[\left(1+k_L\right) \cdot \left(\boldsymbol{A}_l \nu_l + \ddot{\Delta}\mathbf{x}_{d.il} - \varepsilon_{il} \right) + \right.$$
$$+ \sum_{j \neq i,l}^{N} \left(\boldsymbol{A}_j \nu_j + \ddot{\Delta}\mathbf{x}_{d.ij} - \varepsilon_{ij} \right) - \Lambda \mathrm{sat}\left(\frac{\mathbf{s}_{i,F}}{\Phi} \right) -$$
$$\left. -2\left(N-1+k_L\right) \dot{w}_{max} \mathrm{sgn}\left(\mathbf{s}_{Fi}\right) \right], \tag{22}$$

where the l is leader vehicle index and k_L the leader additional gain.

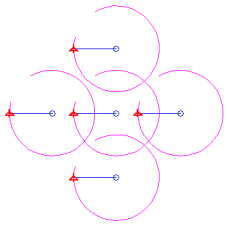

Fig. 4: Earth-aligned formation frame. Cross shaped formation.

C. Earth-aligned formation frame

When the formation frame is permanently aligned to the Earth frame (fig. 4) the desired positions are defined by:

$$\mathbf{x}_{d.i}^{E} = \mathbf{x}_{d.i}^{F} - \mathbf{x}_{d.Lead}^{F} + \mathbf{x}_{Lead}^{E}, \tag{23}$$

where the superscripts E and F indicate if the vectors are described in the Earth or Formation frames, respectively. $\mathbf{x}_{Lead}$ and $\mathbf{x}_{d.Lead}$ are the leader current position and desired formation position. As the formation frame doesn't rotate, the desired relative positions remain constant and $\dot{\Delta}\mathbf{x}_{d.ij} = \ddot{\Delta}\mathbf{x}_{d.ij} = \dot{\psi}_{ij} = 0$. The equations in (12) can be simplified to

$$\dot{\mathbf{e}}_{ij} = \dot{\mathbf{x}}_i - \dot{\mathbf{x}}_j,\ \ddot{\mathbf{e}}_{ij} = \ddot{\mathbf{x}}_i - \ddot{\mathbf{x}}_j \tag{24a}$$

$$\dot{e}_{x.ij} = \dot{\mathbf{e}}_{ij} \cdot \hat{\mathbf{x}}_{ij},\ \dot{e}_{y.ij} = \dot{\mathbf{e}}_{ij} \cdot \hat{\mathbf{y}}_{ij} \tag{24b}$$

This kind of formation produces the same path for every UAV with a constant positional offset. This may be useful to maintain a constant spatial sampling over time.

D. Path-aligned formation frame

Most aircraft formations align their frame with the flight path. The most simple implementation maintains a constant formation shape, rotating it with the path direction (fig. 5). In these formations the shape base coordinates defined by

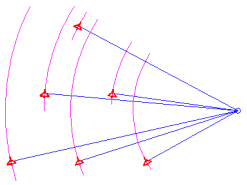

Fig. 5: Path-aligned formation frame with fixed formation frame. Arrow shaped formation.

operator ($\mathbf{x}_{i.F}$) are rotated with the path heading and serve as inputs for the formation internal velocities and accelerations:

$$\mathbf{v}_{Fi}^{E} = \boldsymbol{R}_{\psi_F}^{-1} \begin{bmatrix} -y_{i.F} \\ x_{i.F} \end{bmatrix} \dot{\psi}_F \tag{25a}$$

$$\mathbf{a}_{Fi}^{E} = -\boldsymbol{R}_{\psi_F}^{-1} \mathbf{x}_{i.F} \dot{\psi}_F^2 \tag{25b}$$

Instead of maintaining fixed formation positions, the formation may also adapt to the required kinematics, i.e., when the trajectory is curved the base Cartesian coordinates are transformed to polar coordinates (fig. 6). The alignments in

x cease to be a straight line to become the curve followed by the UAVs. In the same way, the y alignments are still straight lines, but not parallel to each other. All y alignment lines now cross the path's center of rotation. The base coordinates become new coordinates $\mathbf{x'}_{i.F}$ on the formation reference frame. These are defined by three new polar coordinates: the formation radius of curvature r_F, defined in this case by the leader radius of curvature and its position on the formation, the UAV i radius of curvature r_i, and the UAV heading differential $\psi_{i.F}$,

$$r_L = \frac{V_{L.infty} * V_{L.gnd}}{g \tan \phi_L} \tag{26a}$$

$$r_F = r_L + y_{L.F},\ r_i = r_F - y_{i.F} \tag{26b}$$

$$\psi_{i.F} = \frac{x_{i.F}}{r_F}. \tag{26c}$$

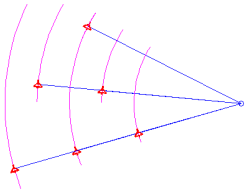

Fig. 6: Path-aligned formation frame with adapting formation frame. Arrow shaped formation.

These result in the subsequent velocities and accelerations relative to the formation frame:

$$\mathbf{x'}_{i.F} = \begin{bmatrix} r_i \sin \Delta\psi_{i.F} \\ y_{i.F} + r_i \left(1 - \cos \Delta\psi_{i.F}\right) \end{bmatrix} \tag{27a}$$

$$\mathbf{v}^E_{Fi} = \boldsymbol{R}^{-1}_{\psi_F} \begin{bmatrix} -y'_{i.F} \\ x'_{i.F} \end{bmatrix} \dot{\psi}_F,\ \mathbf{a}^E_{Fi} = -\boldsymbol{R}^{-1}_{\psi_F} \mathbf{x'}_{i.F} \dot{\psi}^2_F. \tag{27b}$$

III. Simulation results

A. Simulation setup

To test the formation control method we use an extended unicycle aircraft model in a 3 DOF simulation. The formations are composed of a leader and any number of followers. The simulated UAVs are restricted to a range of speeds between 18 and 25 meters per second, and to a maximum bank angle of 25 degrees. The controller parameters are set to control UAVs with a wingspan of 2.5 meters, with a *safety distance* of 5 meters.

We tested formations with shapes like crosses, arrows, and in-line formations. We simulated several initial conditions. The simplest scenario featured every aircraft starting on their intended formation positions, to test the formation position tracking. In another scenario the aircraft started on positions symmetric relative to the desired ones. This tested the formation form-up feature and how well the system handled scrambled initial aircraft positions.

The simulation incorporates perturbations as wind and positional errors. The wind is simulated with steady flow and gusts, i.e., air flow speed and direction variations about

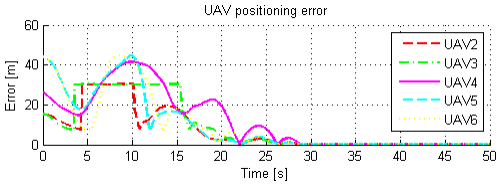

(a) Formation position error.

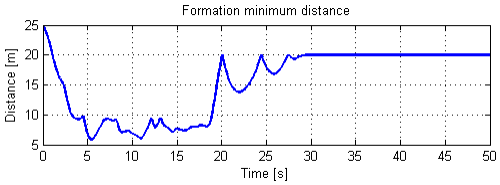

(b) Minimum distance among all aircraft in the formation.

Fig. 7: Simulation data where the follower aircraft start at a opposite positions to the desired ones relative to the leader

the steady flow. These variations are simulated by a Gauss-Markov Process. All the simulations results shown below included wind perturbations, with 16-knot of mean wind and gusts up to 8-knot. Every aircraft was subject to the same steady wind and completely independent gusts, to simulate a worst case scenario.

The positional perturbations were always applied to a single aircraft. We chose this one to be the follower furthest ahead in the formation, to create a string perturbation on the aircraft behind.

B. Results

The simulations show that the system performs well, even with wind and positional perturbations. The formations commanded had minimum distances among UAVs of 20 meters, which presented an additional challenge to the control system. The UAVs converge to the desired formation even if in the initial condition their positions are scrambled. Figure 7a shows the position convergence of a simulation where the follower aircraft started at symmetric positions relative to the ones desired around the leader, i.e., $\mathbf{x}_{Initial.Foll_i} - \mathbf{x}_{Initial.Lead} = \mathbf{x}_{d.Lead} - \mathbf{x}_{d.Foll_i}$. The illustration shows the aircraft settling in the desired formation positions after 50 seconds. Figure 7b illustrates the minimum distance evolution on the same simulation. The minimum distance among UAVs is usually larger than 10 meters. It was driven below 10 meters only when the initial conditions had the aircraft scrambled. The minimum distance very rarely went below the *safety distance* of 5 meters, which only happened when the UAVs were started in very close positions and with conflicting headings.

After forming up the position error is kept low. It only grows slightly if the leader turns too tightly. As such, the minimum distance among the aircraft rarely decreases below one meter from the commanded. When the aircraft converge to their formation positions the average positional error is 0.76 meter with 0.41 meters of standard deviation, even with independent air flow perturbations. If we take away the wind

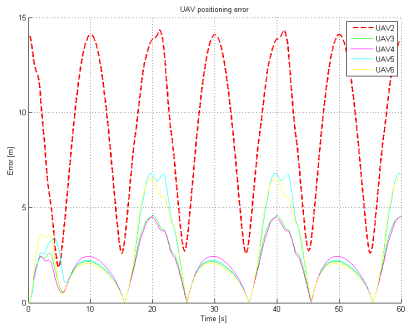

Fig. 8: Mesh stability - The UAVs were set on an "arrow" shaped formation. Attenuation of perturbations from UAV 2 to the other UAVs. UAV 2 presented a sinusoidal motion perturbation. UAVs 3 to 6 show perturbations with reduced amplitude when compared to UAV 2.

variation compensation (18), i.e., set $\dot{w}_{max} = 0m/s^2$ the positional error is still small, with an average of 1.27 meters and 1.40 meters of standard deviation.

The string and mesh stability about the desired formation positions was tested by the generation of step and sinusoidal positional perturbations. The results show that the motion perturbation is attenuated among the formation. Figure 8 shows the positional errors of all the follower UAVs with a sinusoidal perturbation of UAV 2 position. As desired UAV 2 presents the largest positional errors. Figure 8 shows the results of a diagonal sinusoidal perturbation on an "arrow" formation, demonstrating mesh stability.

IV. CONCLUSIONS AND FUTURE WORK

A. Conclusions

We developed a formation flight control system suitable to control fixed wing aircraft. The method handles every phase of the formation maneuver including the initial position convergence (form-up) and the formation shape tracking. To form-up safely with the aircraft starting from any position the system includes a collision avoidance feature. Further, this feature allows a safe control of close formations, as shown by the results. This algorithm was intended to control small UAVs, and the results show that the UAVs very rarely come closer than the 5-meter *safety distance*. The control system handles the air flow perturbations and the formation vehicles' positional perturbation well. It keeps the positional error under 2 meters, even with gusts up to 8 knots. The individual vehicle positional error is attenuated over the formation, showing good string and mesh stability.

B. Future Work

Currently the control method is being adapted to a dynamic model, instead of the kinematic used in this paper. The system is also being tested with a 6 DOF simulation, more closely reproducing the UAV dynamics. Further, the alternative *leaderless formation* version is under development. This should be a better solution for a distributed control scheme. The *leaderless formation* allows the application of predictive dynamic models to compensate for the communication delays and losses. We also intend to prove that the system is mesh stable. Further, we intend to verify the controller properties under wind perturbations, communication delays, and sensor noise. Another important issue is the definition of a set of initial conditions for which no collisions occur.

V. ACKNOWLEDGMENTS

We gratefully acknowledge the support of the AsasF group and the researchers from the Underwater Systems and Technology Laboratory, from the University of Michigan ARC Lab, and from the Portuguese Air Force Academy.

REFERENCES

[1] D. Swaroop and J. K. Hedrick, "String stability of interconnected systems," *Automatic Control, IEEE Transactions on*, vol. 41, pp. 349 –357, Mar. 1996.

[2] C. N. Phana and H. H. Liu, "Dynamic mapping of forest fire fronts using multiple unmanned aerial vehicles," in *AIAA Guidance, Navigation, and Control Conference*, (Toronto, Ontario, Canada), Aug. 2-5 2010.

[3] M. V. Ramana, V. Ramanathan, D. Kim, G. C. Roberts, and C. E. Corrigan, "Albedo, atmospheric solar absorption and heating rate measurements with stacked uavs," *Quarterly Journal of the Royal Meteorological Society*, no. 133, pp. 1913–1931, 2007.

[4] M. J. Vachon, R. J. Ray, K. R. Walsh, and K. Ennix, "F/A-18 aircraft performance benefits measured during the autonomous formation flight project," in *AIAA Atmospheric Flight Mechanics Conference and Exhibit*, (Monterey, California), Aug. 5-8 2002.

[5] J. M. Fowler and R. D'Andrea, "Distributed control of close formation flight," in *Proceedings of the 41st IEEE Conference on Decision and Control*, vol. 3, (Las Vegas, Nevada, USA), pp. 2972 – 2977, December 2002.

[6] K. Kondak, M. Bernard, F. Caballero, I. Maza, and A. Ollero, "Cooperative autonomous helicopters for load transportation and environment perception," in *Advances in Robotics Research* (T. Kröger and F. M. Wahl, eds.), pp. 299–310, Springer Berlin Heidelberg, 2009.

[7] I. Maza, K. Kondak, M. Bernard, and A. Ollero, "Multi-uav cooperation and control for load transportation and deployment," *Journal of Intelligent & Robotic Systems*, vol. 57, pp. 417–449, 2010.

[8] D. J. Lee, K. Y. Kam, I. Kaminer, D. P. Horner, A. Healey, S. P. Kragelund, K. Andersson, and K. D. Jones, "Wireless communication networks between distributed autonomous systems using self-tuning extremum control," in *AIAA Unmanned Unlimited Conference*, (Seattle, Washington), April 6-9 2009.

[9] Z. Zheng, S. C. Spry, and A. R. Girard, "Leaderless formation control using dynamic extension and sliding control," in *17th IFAC World Congress*, (Seoul, Korea), July 6-11 2008.

[10] F. Sharifi, B. W. Gordon, and Y. Zhang, "Decentralized sliding control of cooperative multi-agent systems subject to communication delays," in *AIAA Guidance, Navigation, and Control Conference*, (Toronto, Ontario, Canada), Aug. 2-5 2010.

[11] Y. Gu, B. Seanor, G. Campa, M. R. Napolitano, L. Rowe, S. Gururajan, and S. Wan, "Design and flight testing evaluation of formation control laws," *IEEE Transactions On Control Systems Technology*, vol. 14, pp. 1105–1112, Nov. 2006.

[12] S. Leven, J.-C. Zufferey, and D. Floreano, "Dealing with mid-air collisions in dense collective aerial systems," *Journal of Field Robotics*.

[13] S. Waydo, J. Hauser, R. Bailey, E. Klavins, and R. Murray, "UAV as a reliable wingman: A flight demonstration," *Control Systems Technology, IEEE Transactions on*, vol. 15, pp. 680–688, july 2007.

[14] C. Tomlin, G. J. Pappas, and S. Sastry, "Conflict resolution for air traffic management: A study in multiagent hybrid systems," *IEEE Transactions on Automatic Control*, vol. 43, pp. 509–521, April 1998.

[15] D. Swaroop, J. K. Hedrick, C. C. Chien, and P. Ioannou, "A comparision of spacing and headway control laws for automatically controlled vehicles," *Vehicle System Dynamics: International Journal of Vehicle Mechanics and Mobility*, vol. 23, no. 1, pp. 597–625, 1994.

[16] M. J. Allen, J. Ryan, C. Hanson, and J. Parle, "String stability of a linear formation flight control system," in *AIAA Guidance, Navigation, and Control Conference and Exhibit*, (Monterey, California, USA), Aug. 5-8 2002.